<Original Article>

The Role of MreB in Intrabacterial Nanotransportation System for Cholera Toxin in *Vibrio cholerae*

Shouichi TAKAYAMA, Hong WU, Shoichi SAKAGUCHI, Yoshihiko FUJIOKA,
Youichi SUZUKI, and Takashi NAKANO

Department of Microbiology and Infection Control, Division of Preventive and Social Medicine, Faculty of Medicine, Osaka Medical and Pharmaceutical University, Takatsuki, Osaka 569–8686, Japan

Key words: *Vibrio cholerae*, cholera toxin, intrabacterial nanotransportation system, MreB, immunoelectron microscopy

ABSTRACT

Vibrio cholerae possesses an intrabacterial nanotransportation system (*ib*NoTS) for transporting cholera toxin (CT) from the inner portion toward the peripheral portion of the cytoplasm. This system is controlled by extrabacterial pH and is closely associated with adenosine triphosphate. The transportation routes of *ib*NoTS for CT have not yet been examined in detail. To examine the routes of *ib*NoTS for CT, we demonstrated by immunoelectron microscopy that CT transported by *ib*NoTS localizes closely with the MreB filament in the bacterium, and the MreB filament polymerization inhibitor A22 obstructs *ib*NoTS for CT. The inhibition by A22 was also associated with CT secretion followed by *ib*NoTS inhibition, as determined by enzyme immunoassay. In support of this, we verified by enzyme immunoassay that CT interacted with the MreB filament. These findings indicate that CT along the route of *ib*NoTS is closely associated with the MreB filament. Since these phenomena were not observed in the other filaments, such as the FtsZ filament, we propose that the route of *ib*NoTS for CT is associated with the MreB filament in *V. cholerae*.

INTRODUCTION

Bacterial pathogenic factors such as toxins and colonization factors are produced in the cytoplasm and transported to specific sites where they express their functions and are secreted through a secretion mechanism. Intrabacterial nanotransportation systems are necessary to move these factors. The extrabacterial environment plays an important role in the pathogenicity of microorganisms. Considering gastroenteric infectious diseases, the pH environment of the gastroenteric lumen affects toxin production and excretion in pathogenic bacteria [1–3]. Moreover, toxin transportation within the bacterial cytoplasm is controlled by extrabacterial pH [4–7]. We found that bacteria possess intrabacterial nanotransportation systems (*ib*NoTSs) for transporting toxins and colonization factors, and these *ib*NoTSs are controlled by extrabacterial pH [4–7].

*ib*NoTSs are biological apparatuses that relocate molecules within the cytoplasm in accordance with changes in the extrabacterial environment. Such a system was first discov-

Address correspondence to:
Hong Wu, Department of Microbiology and Infection Control, Division of Preventive and Social Medicine, Faculty of Medicine, Osaka Medical and Pharmaceutical University, 2–7 Daigakumachi, Takatsuki, Osaka 569–8686, Japan
Phone: +81−72−684−7367 Fax: +81−72−684−6517 E-mail: hong.wu@ompu.ac.jp

ered in *Helicobacter pylori* as an extracellular-proton- and UreI-dependent *ib*NoTS for the colonization factor urease [4]. After the discovery of this *ib*NoTS for urease, similar systems for *H. pylori* CagA [5] and VacA [7] were detected in the bacterium. These three *ib*NoTSs are controlled by extracellular acids. Thereafter, *ib*NoTS in *Vibrio cholerae* was discovered as the transportation system for cholera toxin (CT) [6], which is controlled by the extrabacterial alkaline environment. Immunoelectron microscopy studies of *ib*NoTS demonstrate that these systems function in the priming of exotoxins except for *H. pylori* urease into the corresponding secretion machinery in the cell wall [5–7].

In eukaryotic cells, some types of protein are transported between intracellular compartments through vesicles, cytoskeletons, and motor proteins [8, 9]. In the case of the intracytoplasmic transportation proteins, they are translocated through microfilaments [10,11]. In prokaryotic cells, structural fibrous systems such as MreB [12], FtsZ [13], and crescentin [14] have been identified as prokaryotic homologs of actin, tubulin, and intermediate filaments in eukaryotic cells, respectively. We suggested previously that the bacterial cytoskeleton is a possible route of *ib*NoTS [5]. The mechanism underlying molecular relocation via *ib*NoTS has been gradually clarified. Recently, we have demonstrated that the bacterial cytoskeleton is a possible route of *ib*NoTS, as shown by the findings of our studies by immunoelectron microscopy and the freezing and thawing method [15]. By observing the filament in the bacterial cytoplasm, we found that the route of *ib*NoTS for CagA was likely to be associated with the MreB filament, which is a bacterial cytoskeletal filament [16]. In addition, it has been reported that the MreB filament is not associated with *ib*NoTS for urease. In contrast, the route and factors associated with *ib*NoTS for urease, which is an important pathogenic factor associated with the colonization of the gastric mucosa, are associated with the bacterial cytoskeletal FtsZ filament, which is one of the bacterial cytoskeletal filaments, and its eukaryotic homolog is tubulin [13,17].

There have been some reports that the S-benzylisothiourea compound A22 [S-(3,4-dichlorobenzyl)isothiourea] inhibits the polymerization of MreB [18, 19]. A22 was found to induce *Shigella flexneri* to form coccoid cells and markedly decrease the amounts of effectors secreted by coccoid cells compared with those secreted by rod-shaped cells. These findings showed that the maintenance of rod-shaped cells by MreB in *S. flexneri* was essential for the secretion of effectors via the type III secretion system [20]. Moreover, we reported previously that the MreB filament associated with the route of CagA *ib*NoTS was inhibited by A22 [16].

CT production by *V. cholerae* cells is enhanced by their incubation in peptone medium with an alkaline pH, and virulence gene expression is stimulated in the extrabacterial alkaline environment [21,22]. The type-II secretion machinery for CT is also stimulated by the extrabacterial alkaline environment [23] similarly to *ib*NoTS [6]. Furthermore, we found that adenosine triphosphate (ATP) is closely associated with *V. cholerae ib*NoTS for CT [24]. However, the route of *ib*NoTS for CT remains unclear. Since *ib*NoTS is closely associated with toxin excretion, its route may be similar to that for another secretory toxin, CagA of *H. pylori*, in which the MreB filament is associated with the route of *ib*NoTS for CagA [16]. The MreB filament, a cytoskeletal filament of *V. cholerae*, is a possible route of *ib*NoTS for CT.

To clarify whether MreB is associated with *ib*NoTS for CT, in this study, we examined the interaction between CT along the route of *ib*NoTS and the MreB filament with A22 by the freezing and thawing method and contrast-enhanced double-immunostaining electron microscopy.

MATERIALS and METHODS

Bacterial strains and chemicals

The CT-producing laboratory strain of *V. cholerae* (GTC2647) and the CT-negative clinical strain that was confirmed to be negative for the *ctx* gene by polymerase chain reaction (PCR) analysis were used in this study. The bacterial cells were inoculated into heart infusion broth (HIB, Becton, Dickinson and Company, NJ, USA) supplemented with 5 % fetal bovine serum (FBS) and precultured at 37 °C for 3 h with shaking at 30 rpm in the medium (pH 7.4). The bacterial suspensions were then centrifuged at 1,400 × *g* for 10 min. Resulting bacterial pellets were washed in phosphate-buffered saline (PBS, pH 7.2) and collected by centrifugation (1,400 × *g* for 10 min). After washing, the pellets were resuspended in PBS at 1×10^9 bacterial cells/ml. Some samples were supplemented with 9.4 μg/ml S-(3,4-dichlorobenzyl) isothiourea (A22), as described by Iwai *et al*. [18].

The bacterial suspensions treated with or without A22 were centrifuged at 1,400 × *g* for 10 min. The resulting bacterial pellets were incubated in McIlvaine buffer, which is a mixture of 100 mM citric acid monohydrate and 200 mM disodium hydrogen phosphate (pH 7 or 8) at 37 °C for a designated time.

Determination of minimum inhibitory concentration (MIC)

A susceptibility test was performed using broth microdilution methods in accordance with the guidelines established by the Clinical Microbiology Procedures Handbook [25] as described previously [16]. The MIC of A22 in *V. cholerae* was determined by a broth microdilution method using Brucella broth at 37 °C for 24 h. The minimum concentration of A22 required for the conversion of approximately > 80% of the cells from comma-shaped to spherical and larger cells was defined as the minimum spherical- and larger-form-inducing concentration (MSIC) as determined by the MIC test, which was described previously [16]. The formation of spherical and larger cells was observed in the liquid incubation medium in the MIC test using a phase-contrast microscope and an Olympus BH-2 microscope with Gram staining. The MSIC of *V.*

cholerae was defined as the minimum concentration at which fewer comma-shaped cells were detected because the *V. cholerae* cells changed into spherical and larger cells during incubation [26]. The growth of the bacterial cells was also detected on the basis of the turbidity of cultures.

Antibodies

For immunoelectron microscopy, an anti-CTB (B subunit of cholera toxin) rabbit polyclonal antibody of *V. cholerae* (Abcam, Cambridge, UK), an anti-CTB mouse monoclonal antibody (Biogenesis, Poole, UK), and a rabbit anti-FtsZ polyclonal antibody (Cusabio Technology LLC. Houston TX, USA) of *Escherichia coli*, which also recognizes the *V. cholerae* FtsZ (data not shown), were used. A goat anti-mouse IgG antibody labeled with 5-nm colloidal gold particles (hereafter referred to as small particles) and a goat anti-rabbit IgG antibody labeled with 10-nm colloidal gold particles (hereafter referred to as large particles) (EY Laboratories, San Mateo, CA, USA) were used as the secondary antibodies. Because there is no anti-MreB antibody for MreB of *V. cholerae*, the sequence of *V. cholerae* mreB was decoded, and an anti-MreB serum was raised against the component peptide. Keyhole limpet hemocyanin (KLH): JW 13-week-old rabbits were immunized by subcutaneous injections of four antigen solutions (18 mer (CGHAAKQMLGRTPGNISA), 16 mer (CRQVHDNSVLKPSPRV), 19 mer (CEIEVRGRNLAEGVPRSFT), and 19 mer (CARGGGKALEMIDMHGGDL)) five times. The total amount of protein injected was approximately 2 mg/rabbit. Serum samples were collected on the 55th day after the last injection and used as the anti-MreB serum. The entire immunization protocol was performed by Sigma-Aldrich (Tokyo, Japan). The anti-MreB serum was used as the antibody for immunization in the following experiments. The specificity of the antibody was examined by enzyme-linked immunosorbent assay performed by Sigma Aldrich, and we also confirmed that a band specific for *V. cholerae* MreB could be detected by Western blot analysis using the MreB antibody (sera). In addition, the MreB molecule of bacterial cells incubated with or without A22 was detected by immunoelectron microscopy using an anti-MreB antibody (sera) labeled with gold particles, by immunofluorescence microscopy (data not shown), and by enzyme immunoassay (EIA). The MreB–immunogold particles show the localizations of MreB in *V. cholerae*; MreB was observed by double-staining immunoelectron microscopy to be under the cell wall, suggesting a cross section of the helical structure of MreB bundles. The MreB–immunogold particles show that MreB was also associated with the cytoplasmic filamentous structures of *V. cholerae* prepared by the freezing and thawing method and observed by immunoelectron microscopy; this finding is the same as that obtained by Nakano *et al*. [15] using MreB–immunogold particles for immunolabeling MreB in *H. pylori*. It was clarified that the anti-MreB serum was specific to MreB of *V. cholerae* for immunoelectron microscopy. Therefore, the anti-MreB serum was used for immunolabeling in this study. For EIA, a rabbit polyclonal antibody (sera) against *V. cholerae* MreB, a rabbit polyclonal antibody against *E. coli* FtsZ, and the mouse monoclonal antibody against *V. cholerae* CTB were used as the primary antibodies, and a horseradish peroxidase (HRP)-conjugated goat anti-mouse IgG (STR, Victoria, BC, Canada) antibody was used as the secondary antibody.

EIA for CTB

V. cholerae cells were treated with or without A22 prior to exposure to an alkaline buffer (pH 8) at 37 °C for a designated time. The buffer containing the bacterial cells was centrifuged at 1,400 × *g* for 10 min at 4 °C, and the resulting bacterial cell pellet was harvested and lysed by sonication using a CelLytic™ B Plus Kit (Sigma-Aldrich, St. Louis, MN, USA), followed by centrifugation at 10,000 × *g* for 5 min. The supernatant obtained was subjected to antigen-capture EIA of the produced CTB. For the measurement of the secreted CTB, the bacterial cells were treated similarly and pelleted by centrifugation at 1,400 × *g* for 10 min. The supernatant obtained was also subjected to EIA. In the assay, an immunoaffinity-purified rabbit polyclonal antibody (300-fold dilution) against CTB adsorbed to microplates was used. To immobilize the antibody, the microplates were incubated at 4 °C for 24 h. After washing with 0.05 % Tween-20 in PBS (TPBS), Blocker Casein in PBS (Thermo, Tokyo, Japan) was added to the wells to block nonspecific reactions, and then the diluted samples were added to the microplates. The microplates were incubated for 1 h and then washed with TPBS. A 300-fold diluted mouse monoclonal antibody against CTB was added to the microplates, and the microplates were incubated for 1 h at room temperature. After washing the microplates with TPBS, the secondary antibody (a horseradish peroxidase (HRP)-conjugated goat anti-mouse IgG) was added to the microplates, and the microplates were incubated for 1 h at room temperature. The microplates were washed with TPBS to remove any unbound substances, and 2,2'-azino-di-(3-ethyl-benzthiazoline-6-sulfonate) (ABTS; KRL, MD, USA) was added to the microplates prior to incubation for 40 min. A stop solution containing 10 % SDS was added to the microplates, and the absorbance of a sample at 405 nm was measured using a spectrophotometer as described previously [6].

Measurement of MreB–CT interaction in V. cholerae based on EIA

The level of MreB–CT interaction in *V. cholerae* cells that were treated with McIlvaine buffer at pH 5 for designated periods was quantified by EIA. To measure the level of the MreB–CT interaction, the buffer containing *V. cholerae* cells was centrifuged at 1,400 × *g* for 10 min at 4 °C, and the resulting bacterial cell pellet was harvested and lysed by sonication using a CelLytic™ B Plus Kit (Sigma-Aldrich, St. Louis, MN, USA), followed by centrifugation at 10,000 × *g*

for 5 min. The supernatant of the resulting protein lysates was harvested and then prepared for examining the level of MreB–CT interaction in *V. cholerae* by EIA. We utilized microwells coated with the polyclonal anti-*V. cholerae* MreB rabbit antibody (sera) and the polyclonal anti-*E. coli* FtsZ rabbit antibody as a control. The microwells were incubated at 4 oC for 24 h. After washing with TPBS, Blocker Casein in PBS was added to the wells to block nonspecific reactions, and then diluted lysate samples were added to the microwells, which were then incubated for 1 h and then washed with TPBS. A mouse monoclonal anti-CTB antibody was used as a detection antibody. An HRP-conjugated anti-mouse IgG antibody was added to the wells, which was then incubated for 1 h at room temperature. The wells were washed with TPBS to remove any unbound substances. ABTS (KRL, Gaithersburg, MD, USA) was added and the wells were incubated for another 40 min. A stop solution, 10 % sodium dodecyl sulfate (SDS), was added and the absorbance of a sample was measured spectrophotometrically at 405 nm as described previously [17].

Fixation and staining for immunoelectron microscopy

For the analyses of CT and MreB molecular localization in a *V. cholerae* cell, bacterial colonies incubated with or without A22 and treated at different pHs as described above were fixed with 1% glutaraldehyde in 50 mM cacodylate buffer (pH 7.2) at 4 °C for 60 min. To observe the filament structure in a bacterial cell, another sample was subjected to freezing (–80 °C) and thawing (room temperature) before chemical fixation by a conventional method to observe the structure of the MreB filament in bacterial cells, as described previously [15–17]. In previous studies, MreB– or FtsZ–immunogold particles were found to be associated with filamentous structures in the cytoplasm of *E. coli* and *H. pylori* and were observed successfully by immunoelectron microscopy after preparing the samples by the freezing and thawing method, which is suitable for bacterial samples. The fixed bacterial cells were washed five times with 50 mM cacodylate buffer and dehydrated in a graded ethanol series. The samples were embedded in Lowicryl K4M resin (Polyscience, PA, USA) and polymerized in an ultraviolet irradiator (Dosaka EM, Kyoto, Japan) at –30 °C for 2 days and for another 2 days at room temperature. Ultrathin sections (70–80 nm) were sliced using a Reichert-Nissei ultramicrotome (ULTRACUT-N, Nissei Sangyo, Tokyo, Japan) and mounted on a nickel grid (300 mesh) supported by a carbon-coated collodion film as described previously [4].

The ultrathin sections on a grid were treated with 5 % normal goat serum in PBS to block nonspecific reactions. The sections were reacted with drops of the anti-CTB antibody or double stained with a mouse antibody against *V. cholerae* CTB and a rabbit antibody against MreB in sera (primary antibodies), followed by 5-nm colloidal-gold-particle-labeled anti-mouse IgG and 10-nm gold-particle-labeled anti-rabbit IgG-labeled goat antibodies (secondary antibodies) as described previously [4]. Finally, the immunostained sections were subjected to contrast-enhanced staining as described previously [27]. All procedures for contrast enhancement were performed at room temperature.

All the sections were observed under a transmission electron microscope (HT7800 type, Hitachi, Tokyo, Japan). Digital electron micrographs were taken with a CCD camera (XR-81) at a magnification of 5,000−15,000 ×.

Morphometric analyses

The number of immunogold particles associated with CTB from *V. cholerae* cells was counted on the micrographs of a 7–10 × 10^6 nm^2 randomly selected area. This area of a bacterial cell was measured using an image analyzer (Image J NIH. USA). To quantify the distribution of immunogold particles, a bacterial cell was divided into the outer, medium, and inner portions as defined by Hong *et al*. [4,28], and the densities of the particles per square micrometer in these three portions were determined. The principle of dividing a bacterium into three portions was described previously [4,28].

RESULTS

Localizations of CT and MreB

We attempted to clarify whether the route of *ib*NoTS for CT is closely associated with the MreB molecule. To this end, we first examined the localizations of CT and the MreB molecule in bacterial cells treated in an alkaline-pH medium for 5 or 15 min by double-immunostaining electron microscopy, since we previously found that the *ib*NoTS for CT shifts from the cytoplasm to the periphery near the bacterial membrane following an alkaline pH treatment for 5 or 15 min [6]. The colocalization of immunogold-particle-labeled MreB (large particles; arrowheads △) and CT (small particles; arrowheads ▲) was observed in *V. cholerae* treated in the alkaline-pH medium for 5 and 15 min (**Figs. 1a** and **1b**). Although the localization of CT shifted from the cytoplasm to the periphery, near the bacterial membrane, that of MreB did not shift in bacterial cells treated in the alkaline-pH medium for 15 min.

To investigate whether the route of *ib*NoTS for CT was associated with polymerized MreB, A22-treated bacterial cells were treated at the same alkaline pH and the localizations of the CT and MreB were analyzed. To clarify whether *V. cholerae* was susceptible to A22, the MIC of A22 for the bacterium was first determined and was found to be 12.5 μg/ml, which indicates that A22 has antibacterial activity against *V. cholerae*, as reported previously [26]. The MSIC of A22 was 9.4 μg/ml, at which approximately > 80% of the bacterial cells were converted to spherical and larger cells from comma-shaped cells observed by microscopy with Gram staining. The densities of colony-forming units (CFUs) were not significantly different between A22-treated and non-A22-treated *V. cholerae*, as evaluated by Student's *t*-test ($p = 0.06$). A22 at 9.4 μg/ml changed only the morphology of *V. cholerae* but did not inhibit its growth. Then, by culturing *V. cholerae* cells

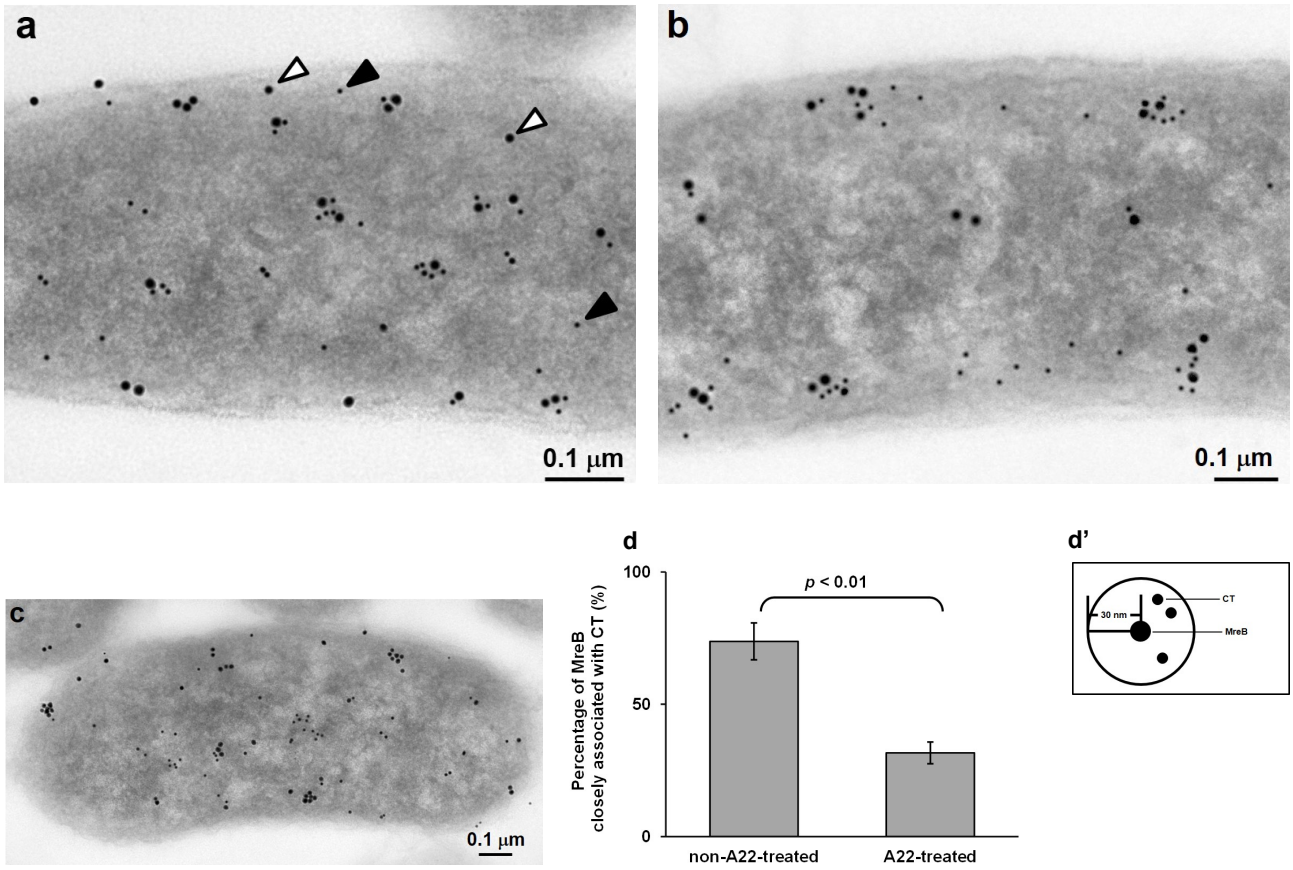

Figure 1 Localizations of *V. cholerae* CT and MreB by double-staining immunoelectron microscopy
Large immunogold particles were associated with MreB and small particles with CT. At 5 (a) and 15 min (b) of alkaline-pH-medium treatment, the CT–immunogold particles in *V. cholerae* were localized close to the MreB–immunogold particles. CT in A22-treated *V. cholerae* was not localized close to MreB compared with that without A22 treatment (c). Arrowheads △ (MreB) indicate large particles and arrowheads ▲ (CT) indicate small particles. Bar = 0.1 μm in all images. Numbers of MreB–immunogold particles in bacteria treated with or without A22 close to CT–immunogold particles (d) ($p = 5.13 \times 10^{-9}$, Student's *t*-test). Among the 400 MreB–immunogold particles, those found within 30 nm from CT–immunogold particles were counted. **d'** is a schematic diagram of the distance between MreB and CT. "●"indicates an immunogold particle.

with the 9.4 μg/ml A22, it was found that the localization of CT in the spherical and larger *V. cholerae* cells was not closely associated with that of MreB (**Fig. 1c**), suggesting that the route of *ib*NoTS for CT was indeed closely associated with polymerized MreB. Among 400 MreB–immunogold particles in bacterial cells treated with or without A22, the number of those found within 30 nm of CT–immunogold particles was counted. It was shown that the number of CT–immunogold particles closely associated with MreB–immunogold particles (**Fig. 1a**) was higher than that of MreB–immunogold particles (**Fig. 1c**), which was significantly different as determined by Student's *t*-test ($p < 0.01$, **Fig. 1d**). **Figure 1d'** is a schematic diagram of the distance between MreB and CT.

To clarify whether *ib*NoTS for CT is inhibited by A22, the spherical and larger *V. cholerae* cells incubated with A22 to obstruct *ib*NoTS for CT were examined. A shift of CT in *V. cholerae* treated in the alkaline-pH medium after incubation with A22 was confirmed by immunoelectron microscopy. CT–immunogold particles (10 nm) seemed to be distributed uniformly across the entire cytoplasm of bacterial cells treated in both neutral- (**Fig. 2a**) and alkaline-pH media for 15 min (**Fig. 2b**). In the non-A22-treated *V. cholerae*, the CT–immunogold particles were distributed uniformly in the entire cytoplasm of *V. cholerae* treated in a neutral-pH medium (**Fig. 2c**) and seemed to be distributed in the periphery, that is, near the bacterial membrane for cells treated in the alkaline-pH medium for 15 min (**Fig. 2d**).

To confirm the shift in localization of the CT–immunogold particles in alkaline-pH-medium-treated bacterial cells incubated with or without A22, the density of CT–immuno-

gold particles was compared with that in neutral-pH-medium-treated cells. The difference in optical density (OD) between the two samples was statistically significant as determined by Student's *t*-test. The densities of CT were not significantly different between the outer and inner portions, between the outer and medium portions, or between the medium and inner portions of the cytoplasm in A22-treated *V. cholerae* at alkaline and neutral pHs (**Fig. 2e**: *n.s.* = not significant, Student's *t*-test). In contrast, the densities of CT were significantly different between the outer and medium portions or between the medium and inner portions of the cytoplasm of *V. cholerae* treated at the alkaline pH (**Fig. 2e**, $p < 0.01$), but those at the neutral pH were not statistically significantly different. These findings indicate that A22 inhibits the peripheral shift of CT in the bacterial cytoplasm and that *ib*NoTS for CT resulting in the shift of CT may depend on polymerized MreB.

Inhibitory effect of A22 on ibNoTS

To determine the effect of A22 on CT secretion and production, which depend on *ib*NoTS for CT, the secretion and production levels of CT were examined by EIA. The secretion level of CT was not increased in the A22-treated bacterial cells (**Fig. 3a**), whereas in non-A22-treated bacterial cells it was increased after a 15-min incubation at the alkaline pH (**Fig. 3b**), in which CT secretion accelerated without the increase in CT production level. The secretion level at the neutral pH did not increase in non-A22-treated and A22-treated *V. cholerae* (**Fig. 3a, 3b**). The production level of CT did not show a delayed increase after a 30-min incubation at the alkaline

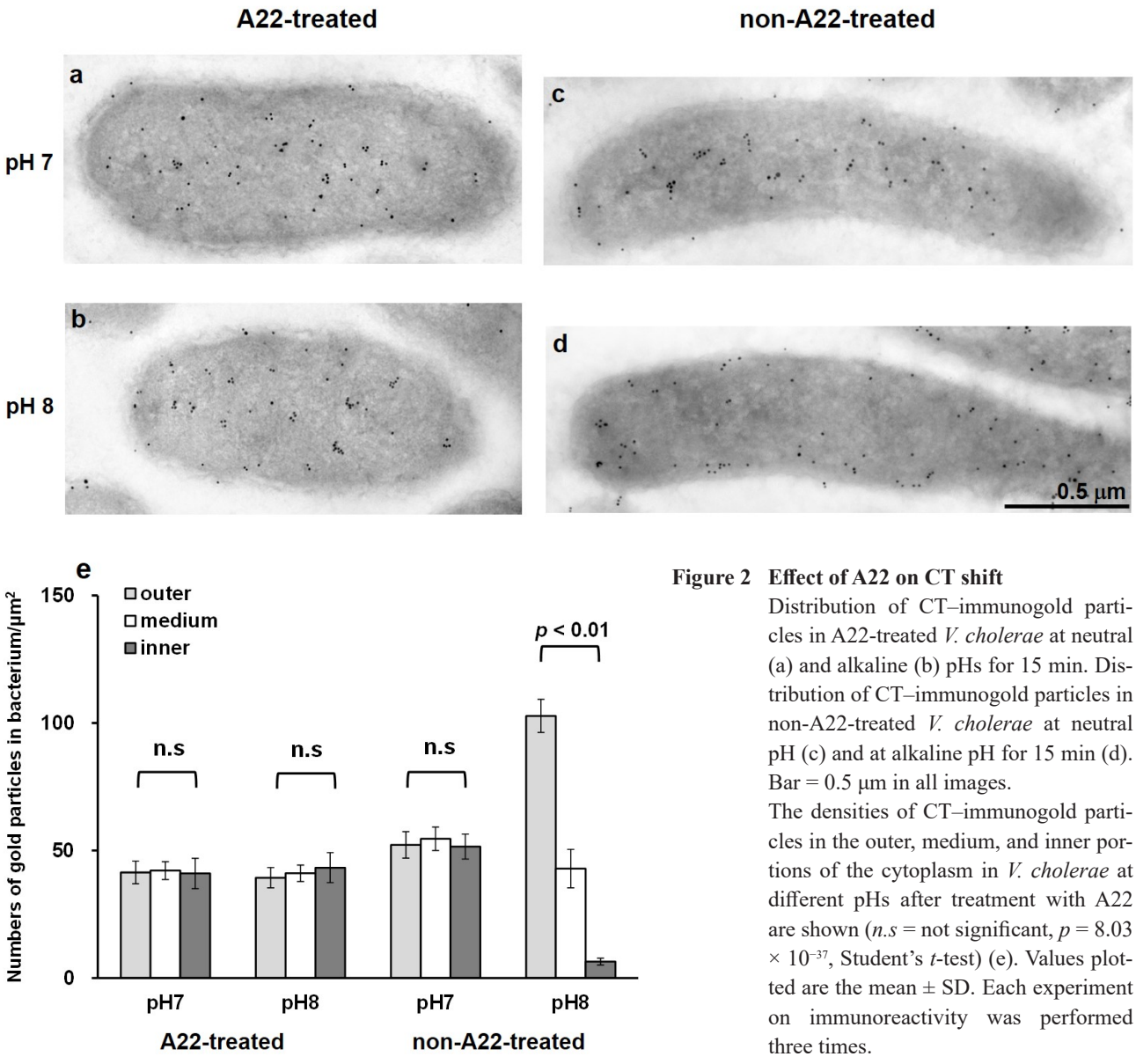

Figure 2 Effect of A22 on CT shift
Distribution of CT–immunogold particles in A22-treated *V. cholerae* at neutral (a) and alkaline (b) pHs for 15 min. Distribution of CT–immunogold particles in non-A22-treated *V. cholerae* at neutral pH (c) and at alkaline pH for 15 min (d). Bar = 0.5 μm in all images.
The densities of CT–immunogold particles in the outer, medium, and inner portions of the cytoplasm in *V. cholerae* at different pHs after treatment with A22 are shown (*n.s* = not significant, $p = 8.03 \times 10^{-37}$, Student's *t*-test) (e). Values plotted are the mean ± SD. Each experiment on immunoreactivity was performed three times.

pH in the A22-treated bacterial cells (**Fig. 3c**), in contrast to that in non-A22-treated bacteria cells which showed a delayed increase of CT production after a 30-min incubation at the alkaline pH owing to the accelerated secretion (**Fig. 3d**). No increase in CT production after a 15-min incubation at the neutral pH was observed in non-A22-treated and A22-treated *V. cholerae* (**Fig. 3c, 3d**). As a result of *ib*NoTS inhibition by A22, the increase in the secretion level of CT was stopped. This phenomenon was examined by EIA. These findings also supported the idea that *ib*NoTS for CT may depend on polymerized MreB.

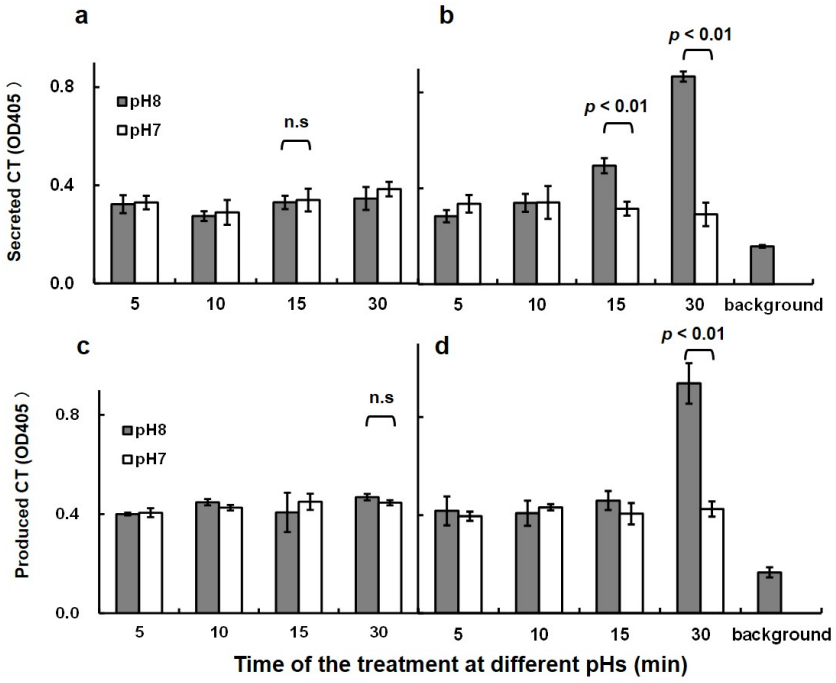

Figure 3 Effect of A22 on CTB secretion and production
The effect of A22 on CTB secretion (a, b) and production (c, d) at pHs 7 and 8 was demonstrated. A22-treated (a and c) and non-A22-treated (b and d) *V. cholerae* cells were examined (*n.s* = not significant, $p = 9.63 \times 10^{-4}$ (15' of b), $p = 2.35 \times 10^{-5}$ (30' of b), $p = 2.77 \times 10^{-4}$ (d), Student's *t*-test). All assays were performed using the same microplate. Values plotted are the mean ± SD from triplicate experiments.

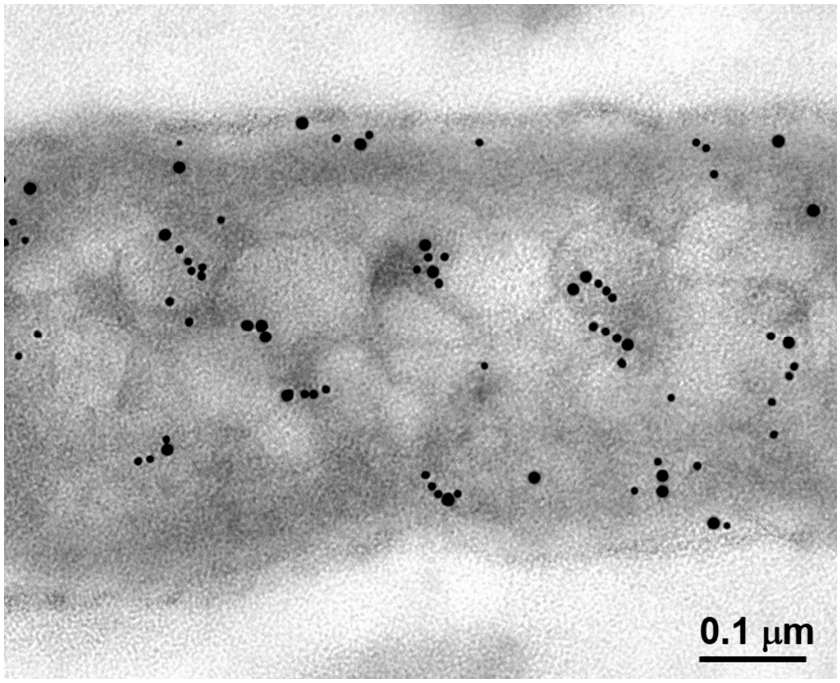

Figure 4 Localizations of CT and MreB in alkaline-pH-treated V. cholerae after freezing and thawing determined by double-staining immunoelectron microscopy
Bar = 0.1 μm.

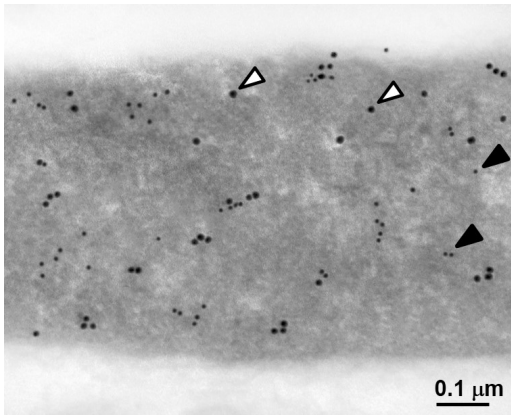

Figure 5 Relationship of the localizations of FtsZ and CT in *V. cholerae* treated at alkaline pH determined by double-staining immunoelectron microscopy
Arrowheads △ (FtsZ) indicate large particles and arrowheads ▲ (CT) indicate small particles. Bar = 0.1 μm.

Localizations of CT and MreB filaments

Since the route of *ib*NoTS for CT is closely associated with the MreB molecule described above (**Fig. 1**), the same samples were examined by the freezing and thawing method, by which the bacterial filament can be observed in the bacterial cytoplasm. The colocalization of immunogold-particle-labeled CT and MreB and their relationship with bacterial filaments were observed to ascertain whether the route of *ib*NoTS for CT is associated with the MreB filament. It was found that some closely colocalized CT– and MreB–immunogold particles were observed in the filaments of *V. cholerae* cells (**Fig. 4**). This finding indicates that the route of *ib*NoTS for CT may be closely associated with the MreB filament in *V. cholerae* cells.

To verify whether the route of *ib*NoTS for CT is closely related specifically to the MreB filament, the relationship of this filament with another filament, the FtsZ filament in *V. cholerae* cells, was investigated. First, the localizations of CT– and FtsZ–immunogold particles were observed. No specific colocalization of FtsZ–immunogold particles (large particles; arrowheads △) and CT–immunogold particles (small particles; arrowheads ▲) was observed in *V. cholerae* treated at an alkaline pH for 5 min when compared with that of CT– and MreB–immunogold particles (**Fig. 5**). These results indicate that FtsZ is not likely to be a molecular scaffold for the route of *ib*NoTS for CT.

To quantitatively validate the stronger association of CT with MreB compared to FtsZ, the colocalization levels were compared statistically. Among 400 MreB– and FtsZ–immunogold particles, the number of those found within 30 nm of CT–immunogold particles was counted. It was shown that the number of CT–immunogold particles closely associated with MreB–immunogold particles (**Fig. 1a**) was higher than that associated with FtsZ–immunogold particles (**Fig. 5**), which was significantly different as determined by Student's *t*-test ($p < 0.01$, **Fig. 6a**). In addition, the density of CT–immunogold particles localized within 30 nm of MreB (FtsZ)–immunogold particles was measured; the density of CT–immuno-

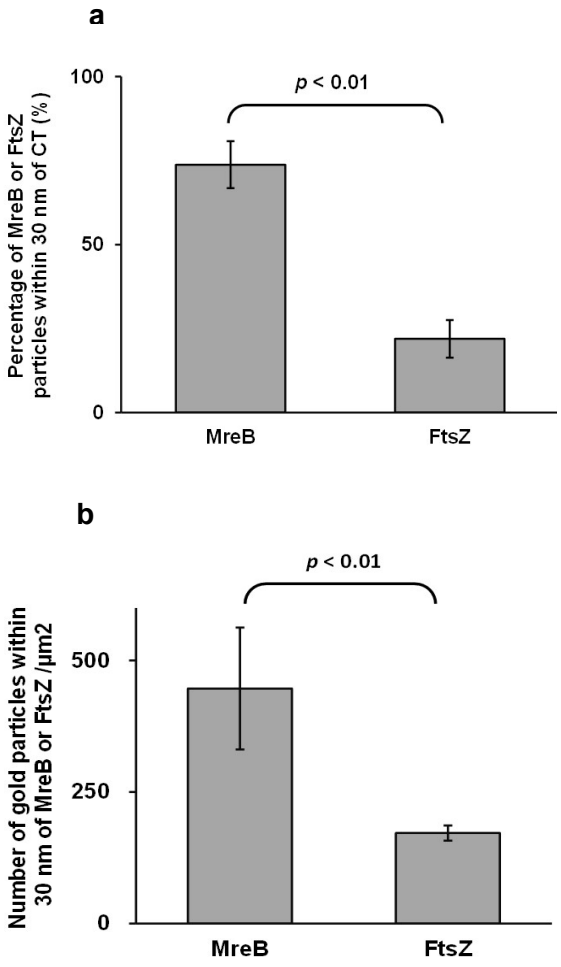

Figure 6 Analysis of localization of *V. cholerae* MreB or FtsZ in relation to CT
a Numbers of MreB– and FtsZ–immunogold particles close to CT–immunogold particles ($p = 1.46 \times 10^{-9}$, Student's *t*-test).
b Density of CT–immunogold particles close to MreB– or FtsZ–immunogold particles ($p = 2.19 \times 10^{-5}$, Student's *t*-test).

gold particles closely associated with MreB–immunogold particles was also significantly higher than that associated with FtsZ–immunogold particles ($p < 0.01$, **Fig. 6b**). The average densities of CT–immunogold particles in the bacterial cells were measured and the difference was insignificant between those of anti-MreB- and anti-FtsZ-antibody-immunostained bacterial cells by Student's *t*-test ($p = 0.34$). This indicates that MreB closely localized with CT but not with FtsZ. The above findings indicate that the route of *ib*NoTS for CT in *V. cholerae* cells is not likely to be a molecular scaffold for the FtsZ filament, but for the MreB filament.

EIA for MreB–CT interaction

We next investigated the molecular association of MreB with CT by biochemical assays. The lysate of *V. cholerae* treated at the alkaline pH was examined by EIA. The MreB–CT complex was first captured by anti-MreB sera, and then CT was detected by using the anti-CTB antibody. The difference in OD between the two patterns of lysate of *V. cholerae* was statistically significant as determined by Student's *t*-test. EIA showed that the amount of CT that interacted with MreB was larger than that of CT in A22-treated bacterial cells and that of CT that interacted with FtsZ ($p < 0.01$; Student's *t*-test), which was first captured by the anti-FtsZ antibody and detected using the anti-CTB antibody (**Fig.7**). **Figure 7'** is a schematic of EIA. The amount of CT interacting with MreB was larger than that of CT in the CT-negative clinical strain ($p < 0.01$; Student's *t*-test). The larger amount of CT interacting with MreB indicated that CT along the route of *ib*NoTS is closely associated with MreB. These findings support that of immunoelectron microscopy observation; MreB in *V. cholerae* cells is likely to be a molecular scaffold for the route of *ib*NoTS for CT.

DISCUSSION

The pathogenesis of many bacterial diseases is explained by the action of exotoxins that are secreted from bacterial cells, such as CagA from *H. pylori* [29,30] and CT from *V. cholerae* [3,31]. Bacterial cells produce exotoxins and transport them to appropriate target molecules of secretion machinery. Therefore, there should be a system in the cytoplasm for the transport of these pathogenic factors. We found some *ib*NoTSs in *H. pylori* for its pathogenesis [4,5,7] and found that the routes of the *ib*NoTSs for CagA and urease were associated with the MreB and FtsZ filaments, respectively [16,17]. The *ib*NoTS for CT was also demonstrated in *V. cholerae* [6]. Furthermore, we found that ATP closely associates

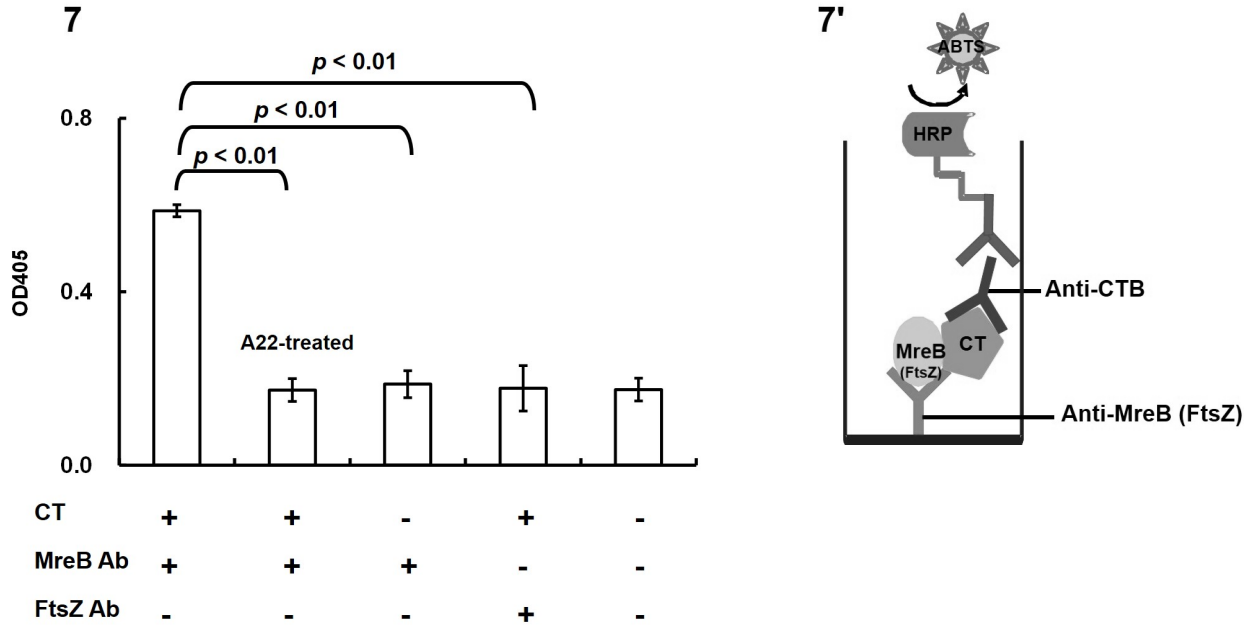

Figure 7 Amount of CT interacting with MreB in lysate of *V. cholerae* determined by EIA.
EIA was performed to examine the amount of CT interacting with MreB in lysate of *V. cholerae*. The amount of CT interacting with MreB in *V. cholerae* treated at an alkaline pH was examined using the rabbit polyclonal anti-MreB serum and mouse monoclonal anti-CTB antibody. 'A22-treated' indicates A22-treated bacterial cells ($p = 8.92 \times 10^{-6}$, Student's *t*-test). As the control, the anti-FtsZ antibody was used instead of anti-MreB serum ($p = 9.88 \times 10^{-5}$), and the CT-negative clinical strain was also used instead of the CT-producing laboratory strain of *V. cholerae* ($p = 1.76 \times 10^{-5}$). **7'** is a schematic of EIA.

with *V. cholerae ib*NoTS for CT [24]. A cytoskeletal filament of *V. cholerae* such as MreB or FtsZ is a possible route of *ib*NoTS for CT, which is a secretion protein similar to CagA of *H. pylori*, but this has not been confirmed in detail. In this study, we found for the first time that CT closely localized with polymerized MreB at the start and terminal points of the route of *ib*NoTS for CT. We also observed by double-staining immunoelectron microscopy that closely localized CT– and MreB–immunogold particles were associated with the MreB filament in *V. cholerae* cells. Moreover, A22 obstructed *ib*-NoTS for CT in *V. cholerae*, as confirmed by immunoelectron microscopy, resulting in a nonincreasing CT secretion level, which was demonstrated by EIA. On the other hand, CT did not closely localize with FtsZ, as determined by double-staining immunoelectron microscopy, which is also among the filaments in *V. cholerae*.

Furthermore, the close relationship between MreB and CT in *ib*NoTS was demonstrated by EIA, in which a large amount of CT colocalizing with MreB was confirmed, which was not observed for CT and FtsZ. These findings indicate that the route of *ib*NoTS for CT is closely associated with the polymerized MreB filament, not with the FtsZ filament.

It has been known that CT is produced in the cytoplasm and transported toward the type-II secretion machinery in the bacterial cell wall by some transport molecules [32]. Here, we have shown that the MreB filament, which exists as a bacterial support structure, is involved in the transport mechanism. The MreB filament, which forms the bacterial cytoskeletal structure [12,33], is considered to support cell shape similarly to the eukaryotic actin fiber, which closely corresponds to the eukaryotic intracytoplasmic transport of proteins. We previously reported that the route of *ib*NoTS for CagA in *H. pylori* was associated with the MreB filament [16]. *V. cholerae* also has a gene homologous to *mreB* and is supposed to have such a cytoskeletal fiber [26]. Taken together, it is highly possible that CT is transported through some proteins interacting with the MreB filament.

Regarding the distribution of the MreB filament, the following observation has been reported multiple studies: rod-shaped bacterial cells have the MreB protein that forms the bacterial cytoskeletal fiber [12,33], and MreB and Mbl molecules form short-pitch helical MreB and MreB that assemble around the middle of a cell [34,35]. There have been many reports on the morphology of polymerized MreB. For example, polymerized MreB has been detected in *E. coli* [36,37], *V. cholerae* [26], and *Bacillus subtilis* [38]. Polymerized MreB localizes in intertwined double helices and band-like structures in various bacteria as determined by fluorescence microscopy. The localization of polymerized MreB was investigated in *B. subtilis* by immunofluorescence microscopy using fluorescent fusion proteins, and polymerized MreB seems to localize near the inner membrane. Some studies showed that the MreB filament also appears similar to MreB patches in *E. coli* and *B. subtilis*, which are dynamic MreB sheets [35,39]. It was also reported that the MreB filament has an appropriate width and length in a bacterial cell [39,40]. However, there are only a few reports on the observation of the structure of MreB in bacterial cells by immunoelectron microscopy. In our previous study of MreB–immunogold particle distribution in *H. pylori* by immunoelectron microscopy, we found that the MreB–immunogold particles reflect the helical shape of MreB bundles/cables/ribbons [15]. They were observed in the bacterial cytoplasm. Thus, these reports also support the idea that the MreB filament might be associated with the route of *ib*NoTS for *V. cholerae* CT.

We have reported an *ib*NoTS-mediated shift of CT to the periphery of the cytoplasm in an extracellular alkaline environment, and we have also demonstrated that CT did not shift at the neutral pH condition [6], which was also observed in our present study. We observed that the route of *ib*NoTS for the alkaline-induced shift of CT is associated with the MreB filament in *V. cholerae*. Since the *ib*NoTS-mediated shift of CT did not occur in the neutral-pH extracellular environment, it was considered that the CT of *V. cholerae* treated at the neutral pH was not associated with the MreB filament. In this study, at the neutral pH, we found that most of the CT was not associated with MreB, as shown by immunoelectron microscopy analysis. In addition, EIA revealed that the CT did not interact with MreB (data not shown).

In eukaryotic cells, cytoskeletal filaments perform important roles in cytoplasmic transportation or in force generation. In prokaryotes, signal recognition particles (SRPs) and SecB mediate the transportation of secretory and membrane proteins to the cytoplasmic membrane [41,42]. Although the signal peptides of prokaryotic proteins associated with these mediators were reported previously [41,43], their routes of transportation are as yet not clarified. Shih and Rothfield [37 anticipated that the cytoskeleton plays important roles in many translocation events in bacteria, since a eukaryotic cell possesses a similar cytoskeletal system for cytoplasmic transportation. We [16,17] hypothesized that *ib*NoTS is associated with filamentous structures of the bacterial cytoplasm in *H. pylori*. Therefore, a cytoskeletal filament of *V. cholerae* is a possible route of *ib*NoTS for CT. In our present study, we found that the route of *ib*NoTS for CT is associated with the MreB filament in *V. cholerae*.

In conclusion, we found that the route of *ib*NoTS for CT was closely associated with the MreB filament. We propose that *V. cholerae* possesses an MreB-regulated *ib*NoTS for CT, not an FtsZ-regulated *ib*NoTS, and the route of *ib*NoTS for CT is the polymerized MreB filament in *V. cholerae*. By clarifying the mechanism of *ib*NoTS for CT including its route, we may find a new target in the development of a prophylactic agent against *V. cholerae* in the intestinal mucosa.

ACKNOWLEDGEMENTS

We thank Emeritus Professor Kouichi Sano of Osaka

Medical and Pharmaceutical University for his advice on our research. We also thank Ms. Yukiko Takada of the Department of Microbiology and Infection Control, Osaka Medical and Pharmaceutical University for her technical help.

REFERENCES

1. Lamers CB. The changing role of H2-receptor antagonists in acid-related diseases. Eur J Gastroenterol Hepatol. 1996;8:S3–7.
2. Gschwantler M, Dragosics B, Wurzer H, Brandstatter G, Weiss W. Eradication of *Helicobacter pylori* by a 1-week course of famotidine, amoxicillin and clarithromycin. Eur J Gastroenterol Hepatol 1998;10:579–82.
3. Sack DA, Sack RB, Nai GB, Siddique AK. Cholera. Lancet 2004;363:223–33.
4. Hong W, Sano K, Morimatsu S, Scott DR, Weeks DL, Sachs G, Goto T, Mohan S, Harada F, Nakajima N, Nakano T. Medium pH dependent redistribution of the urease of *Helicobacter pylori*. J Med Microbiol 2003;52:211–6.
5. Wu H, Nakano T, Daikoku E, Morita C, Kohno T, Lian HH, Sano K. Intrabacterial proton-dependent CagA transport system in *Helicobacter pylori*. J Med Microbiol 2005;54:1117–25.
6. Aoki H, Wu H, Nakano T, Ooi Y, Daikoku E, Kohno T, Matsushita T, Sano K. Nanotransportation system for cholera toxin in *Vibrio cholerae* O1. Med Mol Morphol 2009;42:40–6.
7. Wu H, Nakano T, Matsuzaki Y, Ooi Y, Kohno T, Ishihara S, Sano K. A new type of intrabacterial nontransportation system for VacA in Heicobacter pylori. Med Mol Morphol 2014;47:224–32.
8. Greber UF. Viral trafficking violations in axons: the herpesvirus case. Proc Natl Acad Sci U S A 2005;102:5639–40.
9. Klann M, Koeppl H, Matthias Reuss M. Spatial modeling of vesicle transport and the cytoskeleton: the challenge of hitting the right road. PLoS One 2012;7:e29645.
10. Bohn W, Rutter G, Hohenberg H, Mannweiler K, Nobis P. Involvement of actin filaments in budding of measles virus: studies on cytoskeletons of infected cells. Virology 1986;149:91–106.
11. De BP, Burdsall AL, Banerjee AK. Role of Cellular Actin in Human Parainfluenza Virus Type 3 Genome Transcription. J Biol Chem 1993;268:5703–10.
12. van den Ent F, Amos LA, Lowe J. Prokaryotic origin of the actin cytoskeleton. Nature 2001;413:39–44.
13. Bi EF Lutkenhaus J. FtsZ ring structure associated with divisions in *Escherichia coli*. Nature 1991;354:161–4.
14. Ausmees N, Kuhn JR, Jacobs-Wagner C. The bacterial cytoskeleton: an intermediate filament-like function in cell shape. Cell 2003;115:705–13.
15. Nakano T, Aoki H, Wu H, Fujioka Y, Nakazawa E, Sano K. Fine visualization of filamentous structures in the bacterial cytoplasm. J Microbiol Meth 2003;90:60–4.
16. Wu H, Iwai N, Nakano T, Ooi Y, Ishihara S, Sano K. Route of intrabacterial nanotransportation system for CagA in *Helicobacter pylori*. Med Mol Morphol 2015;48:191–203.
17. Wu H, Iwai, N Suzuki S, Nakano T. Molecular association of FtsZ with the intrabacterial nanotransportation system for urease in *Helicobacter pylori*. Med Mol Morphol 2019;52:226–34.
18. Iwai N, Nagai K, Wachi M. Novel S-benzylisothiourea compound that induces spherical cells in *Escherichia coli* probably by acting on a rod-shape-determining protein(s) other than penicillin-binding protein 2. Biosci Biotechnol Biochem 2002;66:2658–62.
19. Iwai N, Fujii T, Nagura H, Wachi M, Kitazume T. Structure-activity relationship study of the bacterial actin-like protein MreB inhibitors: effects of substitution of benzyl group in S-benzylisothiourea. Biosci Biotechnol Biochem 2007;71:246–8.
20. Noguchi N, Yanagimoto K, Nakaminami H, Wakabayashi M, Iwai N, Wachi M, Sasatsu M. Anti-infectious effect of S-benzylisothiourea compound A22, which inhibits the actin-like protein, MreB, in *Shigella flexneri*. Biol Pharm Bull 2008;31:1327–32.
21. Olson ER. Influence of pH on bacterial gene expression. Mol Microbiol 1993;8:5–14.
22. Matson JS, Withey JH, DiRita VJ. Regulatory networks controlling *Vibrio cholerae* virulence gene expression. Infect Immun 2007;75:5542–49.
23. Sandkvist M, Bagdasarian M, Howard SP. Characterization of the multimeric Eps complex required for cholera toxin secretion. Int. J Med Microbiol 2000;290:345–50.
24. Matsuzaki Y, Wu H, Nakano T, Nakahari T, Sano K. ATP-association to intrabacterial nanotransportation system in *Vibrio cholerae*. Med Mol Morphol 2015;48:225–234.
25. Isenberg HD. Preperation of broth microdilution MIC trays. Clinical microbiology procedures hand book. 2nd Edn. 2004;5.15.
26. Srivastava P, Demarre G, Karpova TS, McNally J, Chattoraj DK. Changes in nucleoid morphology and origin localization upon inhibition or alteration of the actin homolog, MreB, of Vibrio cholera. J Bacteriol 2007;189: 7450–63.
27. Hong W, Morimatsu S, Goto T, Sachs G, Scott DR, Weeks DL, Kohno T, Morita C, Nakano T, Fujioka Y, Sano K. Contrast-enhanced immunoelectron microscopy for *Helicobacter pylori*. J Microbiol Meth 2000;42:121–7.
28. Wu H. Optimum number of bacterial cells for examination of localization of intrabacterial nanotransportation system by semiquantitative immunoelectron microscopy. Bull OMC 2016;62:19–23.
29. Covacci A, Telford JL, Giudice GD, Parsonnet J, Rappuoli R. *Helicobacter pylori* virulence and genetic geogra-

phy. Science 1999;284:1328–33.
30. Backert S, Moese S, Selbach M, Brinkmann V, Meyer TF. Phosphorylation of tyrosine 972 of the *Helicobacter pylori* CagA protein is essential for induction of a scattering phenotype in gastric epithelial cells. Mol Microbiol 2001; 42:631–44.
31. Turnbull PC, Lee JV, Miliotis MD, Still CS, Isaäcson M, Ahmad QS. In vitro and in vivo cholera toxin production by classical and El Tor isolates of *Vibrio cholerae*. J Clin Microbiol 1985;21:884–90.
32. Reichow SL, Korotkov KV, Hol WG, Gonen T. Structure of the cholera toxin secretion channel in its closed state. Nat Struct Mol Biol 2010;17:1226–32.
33. Shaevitz JW, Gitai Z. The structure and function of bacterial actin homologs. Cold Spring Harb Perspect Biol 2010;2:a000364.
34. Jones LJ, Carballido-López R, Errington J. Control of cell shape in bacteria: helical, actin-like filaments in *Bacillus subtilis*. Cell 2001;23:913–22.
35. Celler K, Koning RI, Koster AJ, van Wezel GP. Multidimensional view of the bacterial cytoskeleton. J. Bacteriol. 2013;195:1627–36.
36. Doi M, Wachi M, Ishino F, Tomioka S, Ito M, Sakagami Y, Suzuki A, Matsuhashi M. Demonstrations of the DNA sequence of the MreB gene and of the gene products of the mre region that function in formation of the rod shape of *Escherichia coli* cells. J Bacteriol 1988;170:4619–24.
37. Shih YL, Rothfield L. The bacterial cytoskeleton. Microbiol. Mol Biol Rev 2006;70:729–54.
38. Abhayawardhane Y, Stewart GC. *Bacillus subtilis* possesses a second determinat with extensive sequence similarity to the *Escherichia coli* mreB morphogene. J Bacteriol 1995;177:765–73.
39. Popp D, Narita A, Maeda K, Fujisawa T, Ghoshdastider U, Iwasa M, Maéda Y, Robinson RC. Filament structure, organization, and dynamics in MreB sheets. J Biol Chem 2010;285:15858–65.
40. Soufo CD, Soufo HJ, Noirot-Gros MF, Steindorf A, Noirot P, Graumann PL. Cell-cycle-dependent spatial sequestration of the DnaA replication initiator protein in *Bacillus subtilis*. Dev Cell 2008;15:935–41.
41. Luirink J and Sinning I. SRP-mediated protein targeting: structure and function revisited. Biochim Biophys Acta 2004;1694:17–35.
42. Papanikou E, Karamanou S, Economou A. Bacterial protein secretion through the translocase nanomachine. Nat Rev Microbiol 2007;5:839–51.
43. du Plessis DJ, Nouwen N, Driessen AJ. The Sec translocase. Biochim Biophys Acta 2011;1808:851–65.

Received September 20, 2022
Accepted November 15, 2022